Temperature-Induced Phase Transitions of the Ordered Superlattice Assembly of Au Nanoclusters

Nirmalya Kumar Chaki and Kunjukrishna Pillai Vijayamohanan*

Physical and Materials Chemistry Division, National Chemical Laboratory, Pune 411 008, India

Received: September 21, 2004; In Final Form: November 22, 2004

Superlattices of monolayer protected metallic and semiconducting nanoclusters have attracted significant attention due to their promising applications in nanotechnology. In this paper, we investigate the effect of temperature on the ordered superlattice structure of relatively larger sized Au nanoclusters passivated with dodecanethiol [ca. $Au_{1415}(RS)_{328}$] with the help of in situ temperature controlled X-ray diffraction (XRD) and infrared spectroscopy (IR) in conjunction with thermogravimetric (TG) and differential scanning calorimetric (DSC) analysis. In brief, monolayer protected Au nanoclusters (AuMPC) were prepared by a modified Brust synthesis technique, where dodecanethiol itself acts as both phase transfer and simultaneous capping agent during the reduction process, generating an average particle size of 3.72 ± 0.4 nm after repeated solvent extraction and careful fractionation experiments. These particles are characterized with the help of UV−vis, transmission electron microscopic (TEM), IR, and NMR techniques, where effective capping as well as the superlattice formation on the TEM grid is evident from the combined analysis of these results. In situ low-angle XRD analysis shows that the particles undergo an irreversible phase transition in the temperature range of 100−115 °C, which is also reflected in the data from in situ IR analysis. However, the DSC analysis does not account for this phase transition, although the reversible phase transition due to the alkyl chain dynamics is in good agreement with the previously reported results. These results indicate the formation of temperature-induced, diffusion-limited phase transition involving nonequilibrium fractal structures, which is in good agreement with the previous available theoretical studies. The determination of the temperature window for the stability of these ordered assemblies would be used to understand the effect of thermal stress for device applications.

I. Introduction

Surface passivation of nanoparticles using a monolayer of organic molecules, such as aliphatic thiols, aromatic thiols, and amines, have been extensively used by many groups to control their size dispersion and shape.[1−4] Monolayer protected metallic and semiconducting nanoclusters (MPCs) are considered as artificial building blocks for creating one-, two-, and three-dimensional nanoarchitectures, i.e., superlattices or artificial solids, where several interesting physical phenomena, arising due to quantum effects, could be conveniently investigated.[5−8] In particular, these ordered arrays could result in several novel physical and chemical phenomena due to the collective interactions of these MPCs encompassing several interesting optical, electronic, and magnetic properties.[5−12] For example, low-temperature studies reveal that the "Coulomb blockade effect" especially governs the electron transport in such assemblies, where the individual site energies, coupling strengths, lattice dimensionality, and orders are expected to play crucial roles in the electronic transport and associated long-range resonant energy transfer (LRRT).[13−15,6] More importantly, both classical coupling and quantum coupling are observed in these structures, where the manipulation of interparticle separation between adjacent MPCs triggers a metal−insulator transition.[10,16,17] The unique physical properties of these ordered assemblies are especially promising for several potential applications including the design of multifunctional chemosensors, nucleation control in templated synthesis, optoelectronics, nanocircuit components such as single electron transistors (SET), resonant tunneling devices, molecular switches, quantum dot lasers, quantum cellular atomata (QCA), and simple photonic devices including light-emitting diodes, photovoltaics, etc.[5,6,8,10,13,18]

There have been extensive reports for grooming different types of MPC superlattice structures of both metals and semiconductors, where various effects including particle size and their distribution, length of capping molecules, or several fundamental issues such as nucleation and the growth kinetics on these ordered assemblies have been comprehensively discussed.[1,9−12,19−24] For example, highly ordered, close-packed superlattices have been formed from narrowly size distributed alkanethiol or alkylamine passivated MPCs due to hydrophobic interactions between adjacent hydrocarbon chains, while longer chains have favored long-range ordering due to the enhancement of the interchain interactions.[19,20] Accordingly, Ohara and co-workers have used the Hamaker theory to account for the cluster−cluster interactions in a superlattice structure considering interactions between two finite volume spheres as a function of their separation.[21] In another remarkable study, Landman and co-workers have used molecular dynamics simulations to understand the structure, dynamics, and thermodynamics of these superlattices of smaller MPCs under various conditions, where they have found the interlocking of bundled alkyl chains due to the predominant van der Waals attractions.[22] In particular, their results show that smaller capping length clusters arranged in a bcc superlattice structure can undergo transition to an fcc

* Corresponding author. Telephone/fax: 91-020-25893044. E-mail: viji@ems.ncl.res.in.

10.1021/jp045709x CCC: $30.25
Published on Web 01/20/2005

lattice at higher temperature.[22] Furthermore, they have also shown that longer chain length MPCs have tetragonally distorted fcc structure, where the interlocking of these bundling passivating molecules can be enhanced along the direction of the tetragonal distortion.[22] In a series of studies, Heath and co-workers have shown the detailed phase behavior of two-dimensional monolayers of Ag superlattices (2−7.5 nm diameter) by a pressure−area isotherm in a Langmuir trough to account for the effect of both size and interparticle separation on superlattice structure.[23] More interestingly, they have observed three distinct types of phase behavior, which could be classified in terms of extra classical volume available of the passivating ligands.[23] Another related study by Pradeep and co-workers shows that AgMPCs and AuAg alloy MPC superlattices have distinct liquid phases as observed by X-ray diffraction (XRD) and calorimetric studies; however, they found that AuMPCs were not ideal for superlattice formation.[24] Although there have been extensive reports available on the effect of temperature on the phase transition of Ag or AuAg alloy MPC superlattices, there are no such systematic reports for AuMPCs.[24,25]

In the present study, we report for the first time the effect of temperature on the assemblies of dodecanethiol (DDT) protected Au nanoparticles (ca. 3.72 nm), by means of in situ temperature controlled XRD and IR studies in conjunction with transmission electron microscopy (TEM) and thermogravimetric−differential scanning calorimetric (TG−DSC) studies. Recently, we have reported that these particles have a unique electron transfer property, which can be conveniently used for device applications.[7e] Further, we found that these particles spontaneously form superlattices upon slow evaporation of solvent on solid supports or TEM grids. In situ temperature controlled XRD and IR studies reveal that upon thermal heating these ordered assemblies of AuMPCs transform to a disordered state. We have identified this phenomenon as temperature-induced irreversible phase transitions from ordered to disordered state. We hope that this study will help in understanding the effect of thermal stress on such ordered assemblies of AuMPCs, practically important for nanodevice applications.

II. Experimental Section

(a) Materials. Dodecanethiol (99%), $NaBH_4$, and $HAuCl_4 \cdot 3H_2O$ were obtained from Aldrich, while toluene and acetone, of AR grade from Merck, were used after further purification. In all these experiments, deionized water (16 MΩ) from a Milli-Q system was used.

(b) AuMPC Synthesis. Monolayer protected Au nanoclusters (AuMPCs) were prepared by modified Brust synthesis using DDT as capping agent.[1a,7e] In brief, particles were synthesized in a biphasic mixture of water and toluene (v:v; 1:1; 50 mL each) using a 1:3 mole ratio of gold salt to thiol in an ice bath. The Au salt-to-thiol ratio was kept constant, since the core size is mainly controlled by the Au:thiol stoichiometry. [1a,2] The biphasic mixture under low temperature (ice bath) was stirred for 30 min and subsequently reduced using dropwise addition of 20 mL of 0.1 M aqueous $NaBH_4$ solution. Upon the slow addition of $NaBH_4$, the pale yellow color of gold salt was transformed to reddish violet indicating Au^0 cluster formation, and after rigorous stirring for 3 h, the Au^0 clusters were found to be shifted to the organic phase. After separation of the nonaqueous portion from the aqueous layer, the nonaqueous layer was concentrated under vacuum at 40 °C. This procedure was repeated 10 times to collect a large amount of sample. The dark violet powder from the toluene layer was redisolved in 10 mL of toluene and centrifuged to precipitate the agglomerated or bigger fraction particles. The highly toluene soluble fraction (after centrifugation) was precipitated by the addition of an excess volume of acetone (250 mL). The particles were allowed to settle and excess acetone was decanted to reduce the volume to 20 mL, followed by repeated centrifugation (5 times) and decantation to remove excess unbound thiol and other unwanted reaction byproducts.

(c) Characterization. All the optical measurements were recorded using a Shimadzu, UV-2101 PC spectrophotometer using a quartz cell (10 mm path length), where the spectra were background subtracted using the same solvent. The high-resolution TEM (HRTEM) micrographs of AuMPCs were taken on a Philips CM 20 FEG (HRTEM) instrument operated at an accelerating voltage of 200 kV, whereas the low-resolution TEM measurements were carried out on a JEOL Model 1200EX instrument operated at an accelerating voltage of 120 kV. A drop of highly purified toluene containing nanoparticles was placed on an amorphous carbon-coated (3 nm thick) Cu grid for electron microscopy. After slow evaporation of the solvent at room temperature, the grid was introduced into the electron microscope chamber. An NMR spectrum was recorded on a Bruker DRX 500 MHz in $CDCl_3$ solvent using TMS as an internal standard. X-ray diffraction experiments were performed using a Rigaku Dmax 2500 diffractometer. The system consists of a rotating anode generator with a copper target and a wide-angle powder goniometer, having a diffracted beam graphite monochromator. A Rigaku low−medium temperature attachment was fitted in the goniometer for high-temperature measurements. The maximum temperature that can be reached in this attachment is 300 °C. The generator was operated at 40 kV and 150 mA. All the experiments were performed in the reflection mode. The sample holder was a copper block, and a very thin layer of MPCs was drop-casted on this block. The copper block with the sample was heated at the rate of 2 °C/min. The diffraction pattern was collected while the sample temperature was held constant within 1 °C of the set temperature, and the data were acquired in 5 min. The sample was kept under vacuum during the experiment to avoid thermal degradation. The diffraction data were collected at room temperature and subsequently at various temperatures as mentioned in the text to monitor the change in structure during heating. The TGA-7 unit in the Perkin-Elmer thermal analysis system was used to determine the thermal stability of these MPCs. The samples were heated under flowing nitrogen atmosphere from 50 to 800 °C, with a scanning rate of 5 °C/min, and the resultant weight loss was recorded. The calorimetric measurements were carried out using the DSC-7 unit in a temperature range of −10 to 150 °C. The samples were heated at a rate of 10 °C/min in a nitrogen environment. The instrument was calibrated using standard procedures, but for heating rates other than 10 °C/min, indium was scanned at the required heating rate to determine the instrumental lag and the sample data were corrected accordingly. Room-temperature and high-temperature infrared spectra of these samples were taken using a Perkin-Elmer FTIR spectrometer (Model PC 16) at a resolution of 2 cm^{-1} in the range of 450−4400 cm^{-1}. A total of 32 scans were used for signal averaging. High-temperature spectra were obtained by mounting the sample in the Mettler Toledo FP82HT hot stage and placing it in the sample compartment of FTIR after alignment using red laser light. The sample was heated at the rate of 5 °C/min, and the spectra were collected while the sample temperature was held constant.

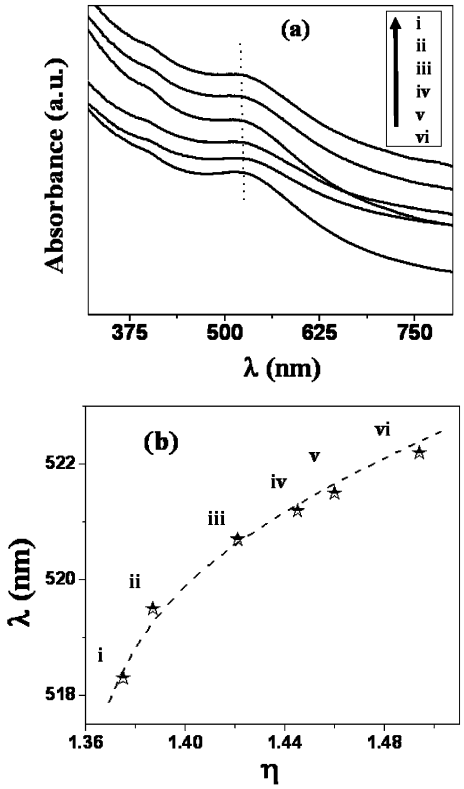

Figure 1. (a) UV−vis absorption of DDT protected Au nanoparticles in hexane, heptane, cyclohexane, chloroform, carbon tetrachloride, and toluene (i−vi). (b) Nonlinear variation of surface plasmon peak position with increase in solvent refractive index.

III. Results and Discussion

The fascinating color of the nanoparticles originates from the interaction of its surface electron with electromagnetic radiation in the UV−vis region, known as surface plasmon resonance.[25] In a remarkable work, Mie solved Maxwell's equation for the absorption and scattering of electromagnetic radiation by spherical particles and found the surface plasmon band position as a function of the dielectric function of the material and its surrounding medium.[25] For example, Figure 1a shows the UV−vis spectra of these particles in various solvents such as hexane, heptane, cyclohexane, chloroform, carbon tetrachloride, and toluene (i−vi), where the absorptions have been shown along the arbitrary *Y*-axis. The surface plasmon resonance of these particles has been observed at 518−522 nm for the above solvents (i−vi), respectively, where the peak position has been red shifted with increase in solvent refractive index. In particular, Figure 1b shows the nonlinear variation of the surface plasmon peak position with the refractive index, which is in good agreement with the earlier reports.[26] However, a minor absorption at ca. 375 nm has been observed, which might be attributed to the presence of weakly bound Au^{3+} ions on these nanoparticles.

Figures 2 and 3 show the TEM images of the highly purified AuMPC fraction along with their statistical distribution as an inset of Figure 3b, which shows a fairly uniform distribution (Gaussian) with an average particle size of 3.72 ± 0.4 nm. The high-resolution images as shown in Figure 2 depict the lattice fringes for these particles. More importantly, the long range ordered superlattice structure is obtained due to the uniform size distribution of these particles (Figure 3a−c). Interestingly, the TEM images of the solid precipitated after mixing a large excess of acetone in the toluene containing AuMPCs show highly ordered superlattice structure along with several multilayer (three-dimensional ordering) structure (Figure 3d). More specifically, these particles show a tendency to arrange in a hexagonal close packed arrangement, where the average particle edge to edge distance is 2.5−2.7 nm. This average spacing is in good agreement with earlier reports, where three to four carbon chains are assumed to be interdigitated during the superlattice formation.[2,24] The composition of these average-size AuMPCs is also approximated from the TEM results by calculating the nearest stable magic numbers as full shell clusters, since certain magic numbers are known to be stable.[27] The average composition of these MPCs is approximated as $Au_{1415}(RS)_{328}$, by assuming the shape of these particles is spherical, the radius of an Au atom is 144 pm, and perfect fcc packing, and further considering two S atoms per three Au atoms on the surface as reported for a two-dimensional self-assembled monolayer.[2,27]

The surface passivation of DDT and the purity of these MPCs have been examined with the help of NMR analysis as shown in Figure 4. The spectrum shows distinct three multiplets corresponding to the protons at C_2, C_{3-11}, and C_{12} carbons at 1.55, 1.26, and 0.84 ppm, respectively. The carbon positions have been marked in the schematic given in the inset. The individual peak positions are similar but broadened compared to those of pure DDT. Interestingly, the proton at the C_1 position is not observed due to the effective capping through the S atom, which causes inhomogeneity in the local chemical environment. In particular, the absence of prominent resonance at 2.7 ppm

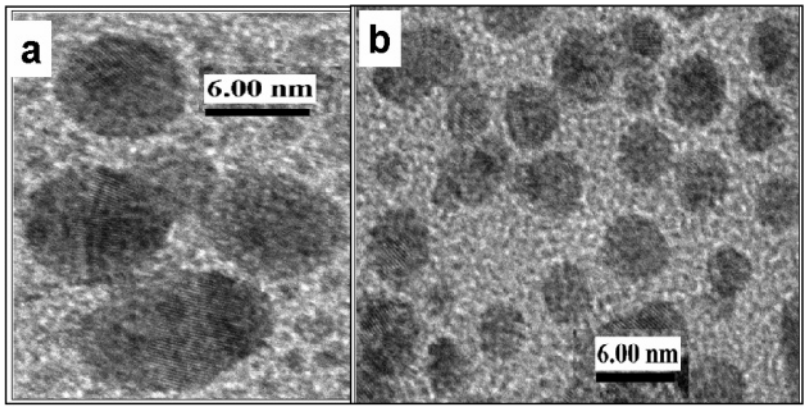

Figure 2. HRTEM images of purified AuMPCs passivated with DDT using repeated solvent extraction and careful fractionation experiments revealing the lattice fringes for these particles.

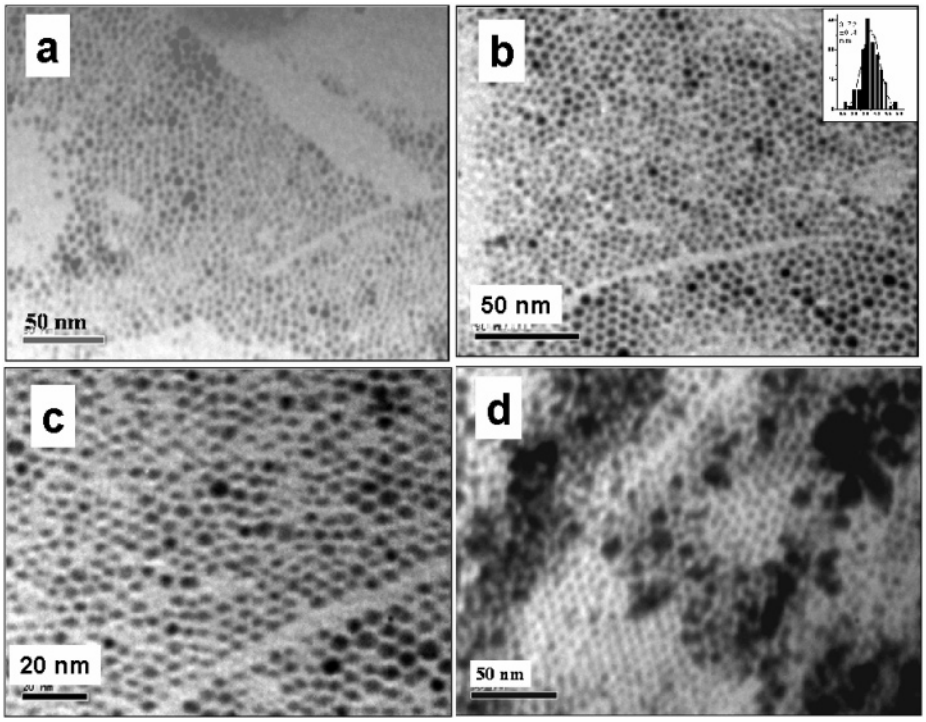

Figure 3. (a−c) Ordered superlattice structures of nearly uniform 3.72 ± 0.4 nm AuDDT particles; (inset) Gaussian distribution of their size. (d) Ordered superlattice structure, along with several multilayer (3D ordering) structures obtained from solid precipitated after mixing large excess of acetone in toluene containing AuMPCs.

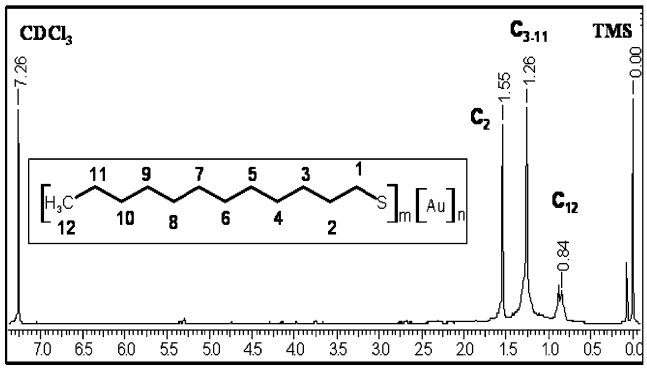

Figure 4. ^{1}H NMR response of purified AuMPC in $CDCl_3$, revealing that the peaks are significantly broadened and shifted from their ideal position due to surface passivation of the Au core.

corresponding to the protons of pure DDT indicates a strong interaction with the metal surface as well as the purity of the sample.

The long-range ordering in these structures could be investigated with the help of low-angle XRD measurement, which could demonstrate the enhanced average *d* spacing. We have used drop-casted thin films of AuMPCs from toluene at room temperature on a Cu substrate for in situ temperature controlled XRD analysis. This AuMPC containing Cu holder was heated at various temperatures, and the XRD data were recorded. For example, Figure 5(i) shows the superimposed variation of the low-angle XRD peaks of these AuMPCs, where several sharp peaks at regular intervals indicate the long-range superlattice formation. The superlattice structure has been indexed in a bcc phase with (110), (220), and (330) lattice planes, which is in good agreement with the previous results.[22b] However, the calculated lattice parameter from low-angle XRD results (ca. 5.25 nm) for the superlattice is smaller than the value obtained from TEM analysis (6.3 ± 1 nm), which indicates that a significant overlap is present between neighboring clusters. More specifically, curves a, b, c, d, e, f, g, h, and i correspond to 25, 65, 85, 115, 125, 150, 165, 180, and 200 °C, respectively, which accounts for a drastic change in the crystallinity of the AuMPC superlattice structure after 110 °C. In particular, the peak positions are almost unaffected for curves a−c, while a shift and an increase in the peak-to-peak spacing are indicated in curve d. Interestingly, curves e−h depict an amorphous nature, which indicate that the crystallinity is lost during 110−120 °C. However, the room-temperature XRD analysis of the previously heated sample at 150 °C retains the amorphous nature, depicting that the transition is irreversible, unlike that of AgMPCs.[24] The thermal stability of these MPCs is also investigated with the help of thermogravimetric (TG) analysis, which shows that partial degradation starts from 175 °C and is complete at 270 °C with almost 20 wt % loss as shown in the inset of Figure 5(i). This weight loss is in good agreement with our approximate calculation of the composition of these MPCs. Further, the TG result also shows that the degradation of these particles is not the reason for the destruction of the superlattice order, which is also confirmed from the higher angle XRD results.

The higher angle XRD results reveal that these MPCs have bulk fcc structure as reported earlier for larger MPCs and the planes are identified as (111), (220), (200), and (311).[1,2] However, Cu sample holder peaks are observed due to the thin nature of the MPC films [marked by asterisks (*) in Figure 5(ii)], although these do not appear in the low-angle region for blank substrate. More importantly, the peak position and the full width at half-maximum of the peaks are not affected up to 165 °C, as shown in Figure 5(ii) corresponding to curves a, b, c, d, e, f, g, h, and i for 25, 65, 85, 115, 125, 150, 165, 180, and 200 °C. However, the intensity of the peaks has been slightly increased above 115 °C and a drastic increment along with sharpening is observed above 180 °C as shown in the inset of Figure 5(ii) for the (111) peak. The sharpening of the peak positions could be attributed to the partial desorption of the thiol monolayers from the nanocluster surface. Thus, these higher angle XRD results

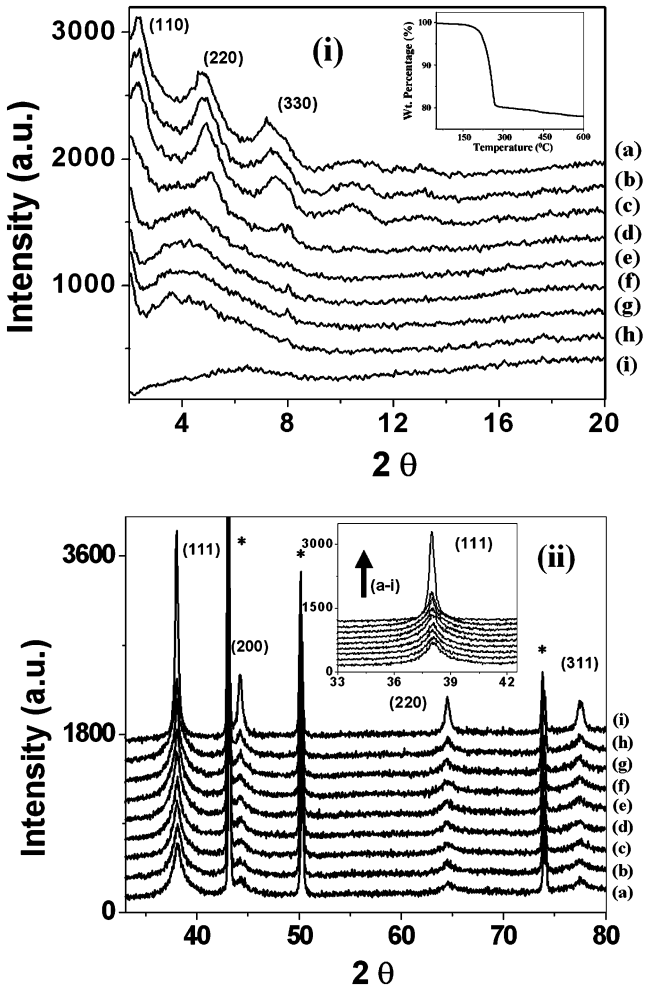

Figure 5. (i) Superimposed variation of low-angle XRD peaks of AuMPCs at (a, b, c, d, e, f, g, h, and i) 25, 65, 85, 115, 125, 150, 165, 180, and 200 °C, respectively, which reveal a sharp phase transition in a temperature range of 110−120 °C; (inset) thermogravimetric (TG) curve of these MPCs. (ii) Superimposed variation of high-angle XRD peaks of AuMPCs at (a, b, c, d, e, f, g, h, and i) 25, 65, 85, 115, 125, 150, 165, 180, and 200 °C, respectively, where the MPCs suggest bulk fcc structure; (inset) effect of temperature for (111) peak.

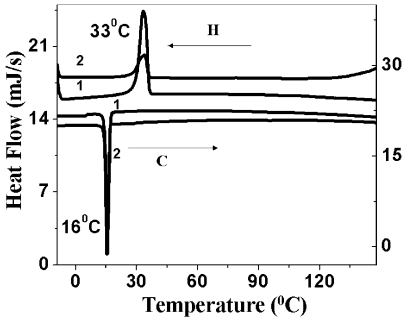

Figure 6. Superimposed first two cycles (1 and 2) of DSC response of AuMPCs. Alkyl chain melting (H) and cooling (C) are seen at 33 and 16 °C, respectively, as reversible first-order transitions.

further preclude the possibility of the destruction of monolayer and increment of the particle size as the reason for the phase transition observed in the low-angle XRD analysis.

In an attempt to capture this phase transition, we have carried out differential scanning calorimetric analysis of purified powders of these samples in the temperature range of −10 to 150 °C. Interestingly, only one distinct first-order transition is observed corresponding to the melting of the alkanethiolate chain assembly, while no other transition is evident, unlike that previously observed for Ag or Au−Ag alloy superstructures and octadecanethiol protected Au MPCs (Figure 6).[24] The alkyl chain melting and cooling are manifested at around 33 and 16 °C, respectively. More importantly, the observed transition temperature has been shifted to higher energy compared to its smaller analogues, as reported earlier, due to the increase in particle size.[2] The reversible hysteresis behavior is a characteristic of the first-order transitions, where during the second cycle the alkyl chain melting transition appears at the same temperature and is comparable to that of the previous cooling curves.[2,24] However, the absence of superstructure phase transition might be attributed to the higher ordering of the alkyl chains as compared to the Ag and Au−Ag alloy.[24] Further heating causes more ordering of the alkyl monolayer as is evident from the increase of the sharpness and the height of these DSC peaks (particularly in the heating curves), which might also suppress the superstructure phase transition.

Variable-temperature infrared analysis was carried out to investigate the exact characteristics of the alkyl chain assembly during the heating. Figure 7(i,ii) shows the high- and low-frequency regions of the infrared spectra of these MPCs in pressed KBr pellets heated in situ at 40, 60, 95, 120, 140, 160, 180, and 200 °C (temperatures correspond to curves a, b, c, d, e, f, g, and h). The positions of the characteristic peaks are drastically shifted to the lower energy side permanently at the higher frequency region above 100 °C. The high degree of conformational order in the monolayer is best evidenced by the position of the symmetric (d^+) and antisymmetric (d^-) CH_2 stretching peaks in the room-temperature IR spectra. Average values of 2852 and 2922 cm^{-1} for these peaks indicate an extremely high percentage of all-trans conformations, characteristic of crystalline alkanes.[24,28] Disordered systems, such as liquid alkanes, display much higher values (2856 and 2928 cm^{-1}, respectively), which have been convoluted to a higher number of gauche defects.[24,28] The r^- band for methylene vibrations has been identified as 2955 cm^{-1}, although the r^+ mode is not prominent enough in the spectra.

All the other bands were assigned on the basis of *n*-alkane vibrations [Figure 7(ii)], where the prominent peaks correspond to methylene wagging and rocking and a large number of progression bands are observed. For the spectrum in the region 1400−1500 cm^{-1}, all-trans scissoring mode has been observed (methylene scissoring (δ) at ∼1460 cm^{-1} and CH_2−S methylene scissoring (δ) at ∼1410 cm^{-1}). The peak at 1376 cm^{-1} is attributed to the symmetric bending vibration of CH_3 groups. The presence of a large number of bands between 1200 and 1400 cm^{-1} corresponds to either twisting−rocking or wagging progression modes, which gives strong evidence for the microenvironment of the alkanethiol monolayer on Au clusters.[24,28] The band at 1341 cm^{-1} in the spectrum is attributed to the end gauche conformation, while the bands at 1125 and 1095 cm^{-1} are assigned as $(c-c)_T$ and $(c-c)_g$ stretching modes, respectively. In particular, these prominent progression bands are indicative for the presence of a higher order in the monolayers such as columnlike, which might be one of the reasons for the absence of superstructure melting in DSC. The 700−800 cm^{-1} region comprises two sets of bands, with the first one due to methylene rocking (726 cm^{-1}) and the other due to C−S stretching.[24,28]

Upon successive heating, interestingly, the high-frequency region shows a drastic change in the symmetric (d^+) and antisymmetric (d^-) CH_2 stretching peaks compared to that of other methylene vibrations. In particular, the CH_2 stretching peaks are found to be shifted to higher values at a temperature

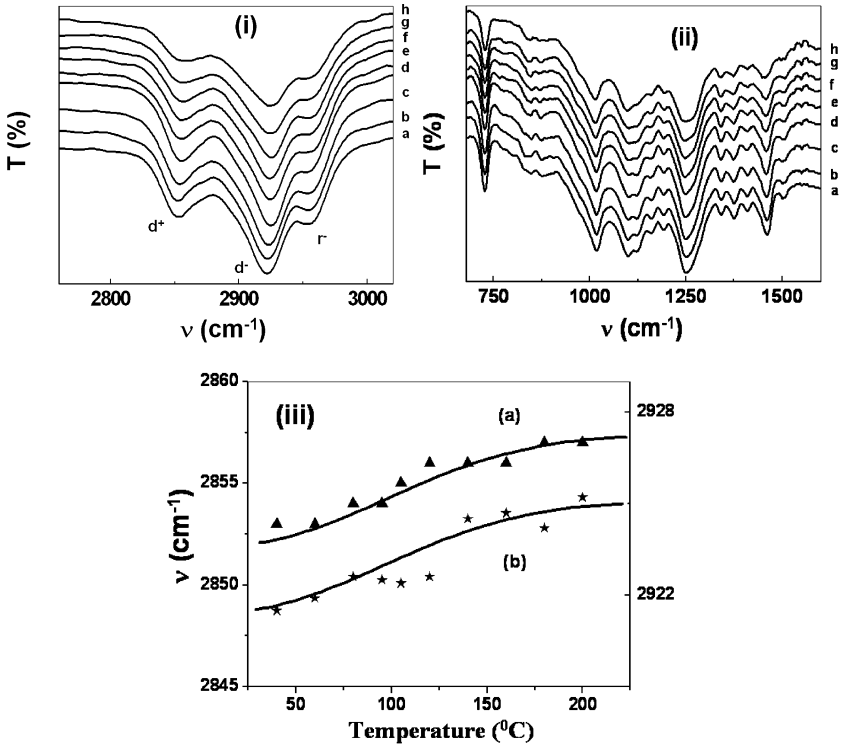

Figure 7. (i and ii) High- and low-frequency regions of infrared spectra of MPCs in pressed KBr pellets heated in situ at 40, 60, 95, 120, 140, 160, 180, and 200 °C corresponding to curves a−h, where positions of characteristic peaks for aliphatic alkane are drastically shifted to lower energy side permanently at higher frequency region above 100 °C. (iii) Variation of symmetric (a) and antisymmetric (b) peak positions with temperature, where the change of the methylene local environment suggests a temperature-induced phase transition.

SCHEME 1: Schematic Representation of Irreversible Phase Transition of AuMPCs from Ordered Assemblies into Disordered State in Accordance with Results of in Situ Temperature Controlled XRD and IR Studies

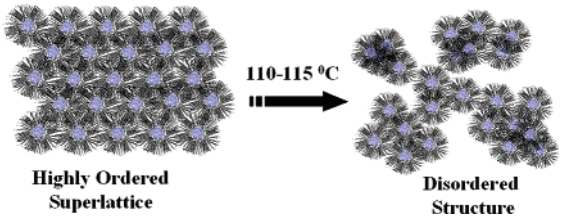

range of 105−120 °C, indicating a disordered system. Figure 7(iii) depicts the variation of symmetric (a) and antisymmetric (b) peak positions with temperature, where the change of the methylene local environment is evident. However, the presence of unaffected progressions bands (1200−1400 cm^{-1}) above the DSC melting temperature suggests a higher order of intrachain packing (can be viewed as bundled columns of alkyl chains[24f]), which increases as a result of repeated annealing. It is also possible that some of these chains near the metal core are not likely to be molten and hence become more ordered during repeated annealing. This clearly suggests that in this temperature range the phase transition of the superstructures happens, which causes destruction of the ordering. In contrast, in the low-frequency region, the C−H stretching does not show any characteristic shift, although partial narrowing of the peaks with heating is observed, indicating increased order in the alkyl chain. However, splitting is not observed in the methylene rocking mode in any of these spectra, which indicates that the interchain interactions are less compared to those previously reported for Ag or Au−Ag alloy MPCs.[24]

The complete characterization of these MPCs shows effective capping of DDT on the particle surface, where the order of the monolayer has been reflected by the NMR, DSC, and IR studies. Further, effective van der Waals attraction among adjacent MPC monolayers causes spontaneous superlattice formation as revealed by these results. In situ temperature controlled low-angle XRD and IR studies indicate irreversible phase transition of these ordered assemblies to a disordered state as shown in Scheme 1, where the alkyl chains are considered as ordered columns along with some disordered chains.[24f] The superlattice stability could be understood well with the help of a model of Ohara and co-workers, where the stability is dependent on the degree of the attractive van der Waals interactions due to the passivated alkyl chain.[21] The attractive potential for this interaction has been given for two finite volume spheres as

$$V(D) = -A_H/12[R/D\{1 + D/2(R_A + R_B)]\} + 1/(1 + D/R + D^2/4R_AR_B) + 2\ln[D\{1 + D/2(R_A + \{R(1 + D/R + D^2/4R_AR_B)\}\}]] \quad (1)$$

A_H is the material-dependent Hamaker constant (=1.95 eV for Au−Au attraction), R_A and R_B are the radii of two particles, A and B, respectively, R is the reduced radius, and D is the separation. Further, $V(D)$ is comparable with kT and it behaves differently at both $D \gg R$ and $D \ll R$ limits. Accordingly, if $V(D) \gg kT$, the enhanced attraction causes aggregation to a nonequilibrium structure (fractal), which is governed by the diffusion limited aggregation model.[21,29] In the present case, the heating causes an increment in the ordering of the passivated monolayers of each MPC, facilitating coalescence with its surrounding neighbors. The attractive force for these small aggregates can overcome the attractive interactions necessary for the superlattice formation, thus leading to the destruction of the superlattice order. The loss of crystallinity has been evident from both the low-angle XRD and IR results, where many subtle changes are observed above 100 °C. Thus our

results are in good agreement with the above theoretical predictions of a temperature-induced, diffusion-limited phase transition involving nonequilibrium fractal structures.

IV. Conclusions

The effect of temperature on AuMPC assemblies has been demonstrated with the help of in situ XRD and IR studies in conjunction with TEM and TG-DSC results. More specifically, these AuMPCs form long-range, ordered assemblies due to the attractive van der Waals interactions among the passivated alkyl chains, which upon heating causes an irreversible phase transition to a disordered state. The low-angle XRD data show disappearance of the Bragg peaks corresponding to the larger unit shell of highly ordered superlattices due to the transition to the disordered state upon heating, whereas the IR studies account for the shift in antisymmetric and symmetric stretching frequencies of the methylene vibrations due to the disordered structure. These results are in good agreement with the theoretical prediction that the increment of attractive interactions could cause formation of diffusion-limited nonequilibrium structures. Our study shows that a decrease of temperature sufficiently below the thermal degradation of monolayer from the surface could cause destruction of these superlattices of Au, thus predicting the effective temperature window for any device application of these artificial solids.

Acknowledgment. N.K.C. gratefully acknowledges the Council of Scientific & Industrial Research (CSIR), New Delhi, for financial support. We are thankful to Mrs. Renu Pasricha of the Center for Materials Characterization for TEM facilities and Mr. E. Boje Gowd and Dr. C. Ramesh of Polymer Science and Engineering Chemistry for TG, DSC, and in situ temperature controlled XRD and IR facilities.

References and Notes

(1) (a) Brust, M.; Walker, M.; Bethell, D.; Schiffrin, D. J.; Whyman, R. *J. Chem. Soc., Chem. Commun.* **1994**, 801. (b) Snow, A. W.; Wohltjen, A. *Chem. Mater.* **1998**, *10*, 947. (c) Vijaya Sarathy, K.; Kulkarni, G. U.; Rao, C. N. R. *Chem. Commun.* **1997**, 537. (d) Vijaya Sarathy, K.; Raina, G.; Yadav, R. T.; Kulkarni, G. U.; Rao, C. N. R. *J. Phys. Chem. B* **1997**, *101*, 9876. (e) Crooks, R. M.; Zhao, M. *Adv. Mater.* **1999**, *11*, 217. (f) Leff, D. V.; Ohara, P. C.; Heath, J. R.; Gelbart, W. M. *J. Phys. Chem.* **1995**, *99*, 7036. (g) Leff, D. V.; Brandt, L.; Heath, J. R. *Langmuir* **1995**, *12*, 4723.

(2) (a) Terrill, R. H.; Postelethwaite, T. A.; Chen, C.; Poon, C. D.; Terzis, A.; Chen, A.; Hutchison, J. E.; Clark, M. R.; Wignall, G.; Londono, J. D.; Superfine, R.; Falvo, M.; Johnson, C. H., Jr.; Samulski, E. T.; Murray, R. W. *J. Am. Chem. Soc.* **1995**, *117*, 12537. (b) Wuelfing, W. P.; Templeton, A. C.; Hicks, J. F.; Murray, R. W. *Anal. Chem.* **1999**, *71*, 4069. (c) Chen, S.; Murray, R. W. *Langmuir* **1999**, *15*, 682. (d) Hostetler, M. J.; Wingate, J. E.; Zhong, C.-J.; Harris, J. E.; Vachet, R. W.; Clark, M. R.; Londono, J. D.; Green, S. J.; Stokes, J. J.; Wignall, G. D.; Glish, G. L.; Porter, M. D.; Evans. N. D.; Murray, R. W. *Langmuir* **1998**, *14*, 17. (e) Templeton, A. C.; Wuelfing, W. P.; Murray, R. W. *Acc. Chem. Res.* **2000**, *33*, 27.

(3) (a) Crispin, X.; Bureau, C.; Geskin, V.; Lazzaroni, R.; Brédas, J. *Eur. J. Inorg. Chem.* **1999**, *1999*, 349. (b) Balogh, L.; Tomalia, D. A. *J. Am. Chem. Soc.* **1998**, *120*, 7355. (c) Yeh, M.; Yang, Y.; Lee, Y.; Lee, H.; Yeh, Y.; Chen-Sheng, Y. *J. Phys. Chem. B* **1999**, *103*, 6851.

(4) (a) Manna, A.; Kulkarni, B. D.; Bandyopadhyay, K.; Vijayamohanan, K.; *Chem. Mater.* **1997**, *9*, 3032. (b) Chaki, N. K.; Sudrik, S. G.; Sonawane, H. R.; Vijayamohanan, K. *Chem. Commun.* **2002**, 76.

(5) (a) Colvin, V. L.; Schlamp, M. C.; Alivisatos, A. P. *Nature* **1994**, *370*, 354. (b) Schmid, G.; Baumle, M.; Greekens, M.; Heim, I.; Osemann, C.; Sawitwoski, T. *Chem. Soc. Rev.* **1999**, *28*, 179. (c) Shipway, A. N.; Katz, E.; Willner, I. *Chem. Phys. Chem.* **2000**, *1*, 18. (d) Mirkin, C. A. *Inorg. Chem.* **2000**, *39*, 2258. (e) Rao, C. N. R.; Kulkarni, G. U.; Thomas, P. J.; Edwards, P. P. *Chem. Soc. Rev.* **2000**, *29*, 27. (f) Schmid, G.; Chi, L. F. *Adv. Mater.* **1998**, *10*, 515.

(6) Collier, C. P.; Vossmeyer, T.; Heath, J. R. *Annu. Rev. Phys. Chem.* **1998**, *49*, 371 and references therein.

(7) (a) Nakanishi, T.; Ohtani, B.; Uosaki, K. *J. Phys. Chem. B* **1998**, *102*, 1571. (b) Chaki, N. K.; Sharma, J.; Mandle, A. B.; Mulla, I. S.; Pasricha, R.; Vijayamohanan, K. *Phys. Chem. Chem. Phys.* **2004**, *6*, 1304. (c) Chaki, N. K.; Aslam, M. Gopakumar, T. G.; Sharma, J.; Pasricha, R.; Mulla, I. S.; Vijayamohanan, K. *J. Phys. Chem. B* **2003**, *107*, 13567. (d) Aslam, M.; Chaki, N. K.; Sharma, J.; Mulla, I. S.; Vijayamohanan, K. *Curr. Appl. Phys.* **2003**, *3*, 115. (e) Chaki, N. K.; Singh, P.; Dharmadhikari, C. V.; Vijayamohanan, K. P. *Langmuir* **2004**, *20*, 10208.

(8) Daniel, M.-C.; Astruc, D. *Chem. Rev.* **2004**, *104*, 293.

(9) (a) Kagan, C. R.; Murray, C. B.; Bawendi, M. G. *Phys. Rev. B* **1996**, *54*, 8633. (b) Guzelian, A. A.; Katari, J. E. B.; Kadavanich, A. V.; Barin, U.; Hamad, K. *J. Phys. Chem.* **1996**, *100*, 7212.

(10) (a) Yin, J. S.; Wang, Z. L. *Phys. Rev. Lett.* **1997**, *79*, 2570. (b) Kim, S.-H.; Medeiros-Ribeiro, G.; Ohlberg, D. A. A.; Williams, R. S.; Heath, J. R. *J. Phys. Chem. B* **1999**, *103*, 10341. (c) Collier, C. P.; Saykally, R. J.; Shiang, J. J.; Henrichs, S. E.; Heath, J. R. *Science* **1997**, *277*, 1978. (d) Markovich, G.; Collier, C. P.; Heath, J. R. *Phys. Rev. Lett.* **1998**, *80*, 3807.

(11) Ahmadi, T. S.; Wang, Z. L.; Green, T. C.; Henglein, A.; El-Sayed, M. A. *Science* **1996**, *272*, 1924.

(12) (a) Tanori, J.; Pileni, M. P. *Adv. Mater.* **1995**, *7*, 862. (b) Lisiek, I.; Pileni, M. P. *J. Phys. Chem.* **1995**, *99*, 5077. (c) Pileni, M. P. *J. Phys. Chem. B* **2001**, *104*, 3358.

(13) (a) Dorogi, M.; Gomez, J.; Osifchin, R.; Andres, R. P.; Reifenberger, R. *Phys. Rev. B* **1995**, *52*, 9071. (b) Amman, M.; Wilkins, R.; Ben-Jacob, E.; Maker, P. D.; Jaklevic, R. C. *Phys. Rev. B* **1991**, *43*, 1146.

(14) (a) Thomas, P. J.; Kulkarni, G. U.; Rao, C. N. R. *Chem. Phys. Lett.* **2000**, *321*, 163. (b) Ancona, M. G.; Kruppa, W.; Rendell, R. W.; Snow, A. W.; Park, D.; Boos, J. B. *Phys. Rev. B* **2001**, *64*, 033408.

(15) Schaaff, T. G.; Shafigullin, M. N.; Khoury, J. T.; Vezmar, I.; Whetten, R. L. *J. Phys. Chem. B* **1997**, *101*, 7885.

(16) (a) Aslam, M.; Mulla, I. S.; Vijayamohanan, K. *Appl. Phys. Lett.* **2001**, *79*, 689. (b) Aslam, M.; Chaki, N. K.; Mulla, I. S.; Vijayamohanan, K.; *Appl. Surf. Sci.* **2001**, *182*, 338. (c) Aslam, M.; Gopakumar, G.; Shoba, T. L.; Mulla, I. S.; Vijayamohanan, K.; Kulkarni, S. K.; Urban, J.; Vogel, W. *J. Colloid Interface Sci.* **2002**, *255*, 79.

(17) Quinn, B. M.; Prieto, I.; Haram, S. K.; Bard, A. J. *J. Phys. Chem. B* **2001**, *105*, 7474.

(18) (a) Arakawa, Y.; Takahashi, T. *Optoelectronics* **1988**, *3*, 155. (b) Ugajin, R. *J. Appl. Phys.* **1994**, *76*, 2833. (c) Orlov, A. O.; Amlani, I.; Bernstein, G. H.; Lent, C. S.; Snider, G. L. *Science* **1997**, *277*, 928. (d) Dabbousi, B. O.; Bawendi, M. G. Onitsuka, O.; Rubner, M. F. *Appl. Phys. Lett.* **1995**, *66*, 1316. (e) Greenham, N. C.; Peng, X. G.; Alivisatos, A. P. *Phys. Rev. B* **1996**, *54*, 17628.

(19) (a) Alvarez, M. M.; Khoury, J. T.; Schaaff, T. G.; Shafigullin, M. N.; Vezmar, I.; Whetten, R. L. *J. Phys. Chem. B* **1997**, *101*, 3706. (b) Lin, X. M.; Wang, G. M.; Sorensen, C. M. *J. Phys. Chem. B* **1999**, *103*, 5488. (c) Lin, X. M.; Jaegar, H. M.; Sorensen, C. M.; Klabunde, K. J. *J. Phys. Chem. B* **2001**, *105*, 3353. (d) Prasad, B. L. V.; Stoeva, S. I.; Sorensen, C. M.; Klabunde, K. J. *Langmuir* **2002**, *18*, 7515.

(20) (a) Heath, J. R.; Knobler, C. M.; Leff, D. V. *J. Phys. Chem. B* **1997**, *101*, 189. (b) Harfenist, S. A.; Wang, Z. L.; Alvarez, M. M.; Vezmar, I.; Whetten, R. L. *J. Phys. Chem.* **1996**, *100*, 13904. (c) Wang, Z. L. *Adv. Mater.* **1998**, *10*, 13. (d) Wang, Z. L.; Harfenist, S. A.; Vezmar, I.; Whetten, R. L.; Bently, J.; Evans, N. D.; Alexander, K. B. *Adv. Mater.* **1998**, *10*, 808. (e) Harfenist, S. A.; Wang, Z. L.; Whetten, R. L.; Vezmar, I.; Alvarez, M. M. *Adv. Mater.* **1997**, *9*, 817. (f) Korgel, B. A.; Fullam, S.; Connolly, S.; Fitzmaurice, D. *J. Phys. Chem. B* **1998**, *102*, 8379. (g) Wang, Z. L.; Harfenist, S. A.; Whetten, R. L.; Bently, J.; Evans, N. D. *J. Phys. Chem. B* **1998**, *102*, 3068. (h) Korgel, B. A.; Fitzmaurice, D. *Phys. Rev. B* **1999**, *59*, 14191.

(21) (a) Ohara, P. C.; Leff, D. V.; Heath, J. R. Gelbart, W. M. *Phys. Rev. Lett.* **1995**, *75*, 3466. (b) Hamaker, H. C. *Physica (Utrecht)* **1937**, *75*, 1058.

(22) (a) Luedtke, W. D.; Landman, U. *J. Phys. Chem.* **1996**, *100*, 13323. (b) Whetten, R. L.; Khoury, J. T.; Alvarez, M. M. Murthy, S.; Vezmar, I.; Wang, Z. L.; Stephens, P. W. Cleveland, C. L.; Luedtke, W. D.; Landman, U. *Adv. Mater.* **1996**, *8*, 428.

(23) Heath, J. R.; Knobler, C. M.; Leff, D. V. *J. Phys. Chem. B* **1997**, *101*, 189.

(24) (a) Sandhyarani, N.; Resmi, M. R.; Unnikrishnan, R.; Vidyasagar, K.; Ma, S.; Antony, M. P.; Selvaam, G. P.; Visalakshi, V.; Kumar, N. C.; Pandian, K.; Tao, Y. T.; Pradeep, T. *Chem. Mater.* **2000**, *12*, 104. (b) Sandhyarani, N.; Pradeep, T.; Chakrabarti, J.; Yousuf, M.; Sahu, H. K. *Phys. Rev. B* **2000**, *62*, 739. (c) Sandhyarani, N.; Pradeep, T. *Chem. Mater.* **2000**, *12*, 1755. (d) Mitra, S.; Nair, B.; Pradeep, T.; Goyal, P. S.; Mukhopadhyay, R. *J. Phys. Chem. B* **2002**, *106*, 3960. (e) Sandhyarani, N.; Pradeep, T.; Antony, M. P.; Selvam, G. P. *J. Chem. Phys.* **2000**, *113*, 9794. (f) Pradeep, T.; Mitra, S.; Nair, A. S.; Mukhopadhyay, R. *J. Phys. Chem. B* **2004**, *108*, 7012.

(25) Harfenist, S. A.; Wang, Z. L. *J. Phys. Chem. B* **1999**, *103*, 4342.

(26) El-Sayed, M. A. *Acc. Chem. Res.* **2001**, *34*, 257.

(27) Templeton, A. C.; Pietron, J. J.; Murray, R. W.; Mulvaney, P. *J. Phys. Chem. B* **2000**, *104*, 564.

(28) Aiken, J. D., III; Finke, R. G. *J. Mol. Catal. A: Chem.* **1999**, *145*, 1.

(29) Hostetler, M. J.; Stokes, J. J.; Murray, R. W. *Langmuir* **1996**, *12*, 3604.

(30) Ball, R. C. *Phys. Rev. Lett.* **1987**, *58*, 274.